Materials Research Proceedings **26** (2023) 641-646 https://doi.org/10.21741/9781644902431-103

Multibody dynamics modeling of drivetrain components: On the caged-roller dynamics of centrifugal pendulum vibration absorbers

Mattia Cera[1,a*], Marco Cirelli[2,b], Luca D'Angelo[1,c], Ettore Pennestrì[1,d] and Pier Paolo Valentini[1,e]

[1]Department of Enterprise Engineering, University of Rome Tor Vergata, Rome, Italy

[2]Department of Mechanical Engineering, University Niccolò Cusano, Rome, Italy

[a]mattia.cera@uniroma2.it, [b]marco.cirelli@unicusano.it [c]luca.dangelo.02@alumni.uniroma2.eu, [d]pennestri@mec.uniroma2.it, [e]valentini@ing.uniroma2.it

Keywords: Centrifugal Pendulum Vibration Absorbers, Multibody Dynamics Contact and Friction Models, Caged-Roller Joint, Higher Path Curvature Analysis

Abstract. Centrifugal pendulum absorbers are passive dampers mainly employed nowadays to attenuate torsional vibrations in modern drivetrains to reduce fuel consumption and CO2 emissions. The absorber is linked to the drivetrain by means of a higher kinematic joint composed of slots and rollers, termed *caged-roller joint*. This work aims to investigate the contact between the rollers and the slots through multibody dynamics simulations. As a result, the sliding between the profiles, usually neglected in the design model of the caged-roller joint, is assessed and an estimate of the power loss is provided.

Introduction

Current trends for internal combustion engines (ICEs) suggest operation just above the idle-speed range to reduce fuel consumption. This generates low-frequency and high-amplitude oscillations. On the other hand, to avoid a drop in performance, high driving torque levels should be ensured. modern drivetrains require more effective torsional vibration isolation. The class of centrifugal dampers constitutes a widespread industrial solution adopted by many car manufacturers [1]. Centrifugal pendulum vibration absorbers (CPVAs) are order-tuned passive devices [2,3]. The absorbers counteract the torsional disturbance through their oscillations along a prescribed path within a centrifugal force field. The distinctive feature of CPVAs is that the absorber frequency of oscillation matches, for any rotor speed, the one of the torque to be damped. This is realized by selecting the absorber center of mass (COM) path curvature according to a design equation termed *tuning condition.* The classical approaches for the study of CPVAs nonlinear dynamics (*e.g.* [4-10]) are based on perturbation methods. To offer holistic modeling of these devices, the dynamic behavior of this device is herein explored through multibody techniques (*e.g.* [11]). The damper architecture herein portrayed is the parallel bifilar pendulum, where the absorbers are constrained to translate w.r.t. the rotor by two higher kinematic pairs, each constituted by a roller mating with two slots, denoted as caged-roller joint [12-14]. The ideal design of the slot profiles, needed as a constraint to enforce the tuning condition, requires the assumption of pure-rolling between the mating elements. However, this condition heavily depends on normal contact force amplitude throughout the absorbers oscillations. Hence, this paper focuses on analyzing the sliding and the power losses estimation due to the contact between the roller and the slot by means of multibody dynamics simulations.

Materials Research Proceedings **26** (2023) 641-646 https://doi.org/10.21741/9781644902431-103

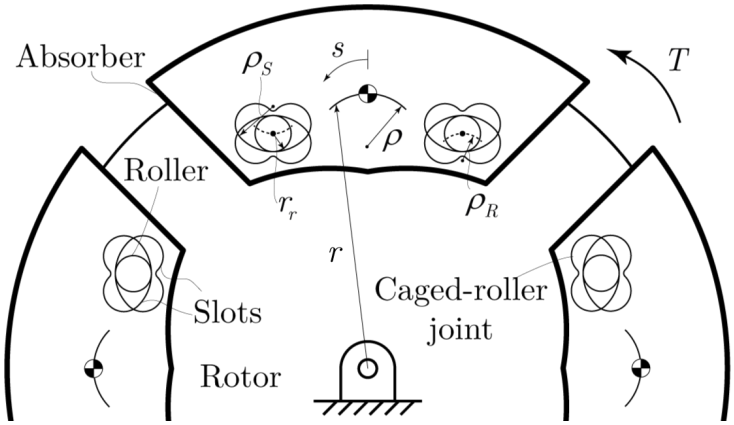

Figure 1: Parallel bifilar CPVA

Damper device modeling

The model kinematic structure is represented in Figure 1 in the reference configuration. Four absorbers of total mass m are linked to the rotor, characterized by a moment of inertia I through eight caged-roller joints. Each one of these joints is composed of a roller and two slots carved on the rotor and on the absorbers, respectively. A 2D circle-to-curve contact is established between the conjugate profiles[1]. The rotor is free to rotate w.r.t. the ground with an initial speed Ω and is subjected to the cubic ramp harmonic torque disturbance:

$$T(t) = T_0 \left[3\left(\frac{t}{t_f}\right)^2 - 2\left(\frac{t}{t_f}\right)^3 \right] \sin n\Theta(t), \tag{1}$$

where Θ is the rotor rotation angle, n is the harmonic order to be damped and t_f is the end-time of the simulation. The CPVA conceptual design is hinged on the following requirements:

- the tuning condition governs the absorber COM path curvature for small oscillations [2-4]:

$$\rho_0 = \frac{r_0}{n^2(1+\sigma)+1}, \tag{2}$$

  where ρ_0 is the absorber COM radius of curvature, r_0 denotes the rotor-absorber COM center distance, the subscript (0) indicates that the variable is evaluated at the reference position, and σ is the detuning, namely the difference between the disturbance and the absorber tuned orders.
- the damper dynamic behavior for large oscillations is controlled by the full absorber COM path. This trajectory, in intrinsic coordinates (ρ, s), is usually selected from the epicycloid family of curves [4-7]:

$$\rho(s) = \rho_0 + \lambda_2 s^2, \tag{3}$$

where s is the absorber curvilinear abscissa and λ_2 is the second curvature ratio of the path $\rho(s)$, which is constant for epicycloids[2]. Since the absorbers undergo a relative translation w.r.t. the rotor, the roller center relative paths (ρ_R, s_R), are obtained by halving Eq.(3):

[1] Contact force models for multibody systems have been analyzed e.g. by Flores [15] and Pereira et al. [16].
[2] For further details on higher path curvature analysis and CPVA design procedures, refer to [4-9,14,17]

Materials Research Proceedings **26** (2023) 641-646 https://doi.org/10.21741/9781644902431-103

$$s_R = \frac{s}{2}, \quad \rho_R = \frac{\rho}{2}, \tag{4}$$

Then, the rotor and absorber slots paths are identical and can be computed as parallel curves of the roller paths (ρ_S, s_S) [14,17]:

$$s_S = s_R\left(1+\frac{r_r}{\rho_R}\right), \quad \rho_S = \rho_R + r_r, \tag{5}$$

where r_r is the roller radius.

The roller-slot contact detection is based on an algorithm with a pre-search to identify contact zones and a detailed-search to find the penetration depth [19]. The contact normal behavior is governed by the Johnson model [16] for the elastic contribution:

$$\delta = \frac{2P(1-\nu^2)}{\pi E}\left[\log\left(\frac{4\pi E\Delta R}{2P(1-\nu^2)}\right)-1\right], \tag{6}$$

where δ is the penetration, P is the load per unit length, $\Delta R = \left(\rho_S - r_r\right)\big|_{s=0} = \frac{\rho_0}{2}$, and (E,ν) are the elastic properties of the steel. This model is fitted with MATLAB fit routine to compute the normal force as follows:

$$F_n = k\delta^{m_1}\left(1+\frac{3}{2}\alpha\dot{\delta}\right), \tag{7}$$

where the damping term $\left(\frac{3}{2}\alpha k\delta^{m_1}\dot{\delta}\right)$ is expressed according to Hunt and Crossley [19] model.

On the other hand, the tangential behavior follows a stick-slip dry friction portrayed in the investigations of Cha et al. [20] and Pennestrì et al. [21]:

$$\begin{aligned} F_t &= \left[\left(1-\beta\right)\mu_\Delta + \mu_v\right]F_n, && v < v_s \text{ (static friction)} \\ F_t &= -\operatorname{sgn}\left(\mu\right)F_n, && v \geq v_s \text{ (dynamic friction)} \end{aligned} \tag{8}$$

This model, and in particular the terms β, μ_Δ, μ_v, μ, depend on five parameters, namely: μ_s, μ_d (static and friction coefficients), v_s, v_d (static and dynamic threshold velocity) and $\Delta_{\max}$ (max stiction deformation). For the further details, refer to the cited works. The data of the system's geometry and inertia, as well as the contact parameters, are reported in Table 1.

Table 1: systems data and parameters

n	σ	λ_2	Ω [rpm]	m [kg]	r_0 [m]	T_0 [Nm]	I [kg m^2]
2	0.01	-0.84	1000	0.3	0.06	21	0.04
k [N/m^m1]	m_1	α	v_s [m/s]	v_d [m/s]	μ_s	μ_d	$\Delta_{\max}$
6.874e9	1.072	0.08	0.15	0.1	0.05	0.04	0.1

Results analysis

The first result needed to assess the CPVA dynamics behavior is the relationship between the torque amplitude and the absorber COM oscillation amplitude, depicted in the plot of Figure 2.

Materials Research Proceedings **26** (2023) 641-646 https://doi.org/10.21741/9781644902431-103

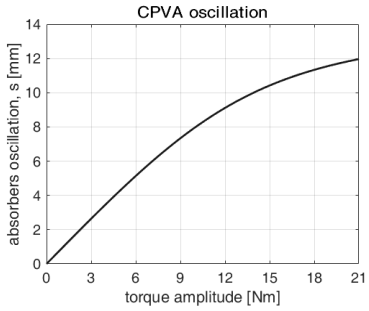

Figure 2: absorber oscillation amplitude .vs. torque amplitude.

For low torque levels, the device response is quasi-linear, whereas for large oscillations the resulting behavior is hardening. This feature depends on the selected value of the curvature ratio λ_2. Then, in Figure 3 are represented the friction coefficient and sliding velocity curves with respect to the torque amplitude. In particular, the gray line is for the interaction between the absorber slot and the roller, whereas the black line is for the rotor slot-roller contact. Moreover, the dashed lines indicate the threshold values v_s, v_d, μ_s, μ_d, respectively.

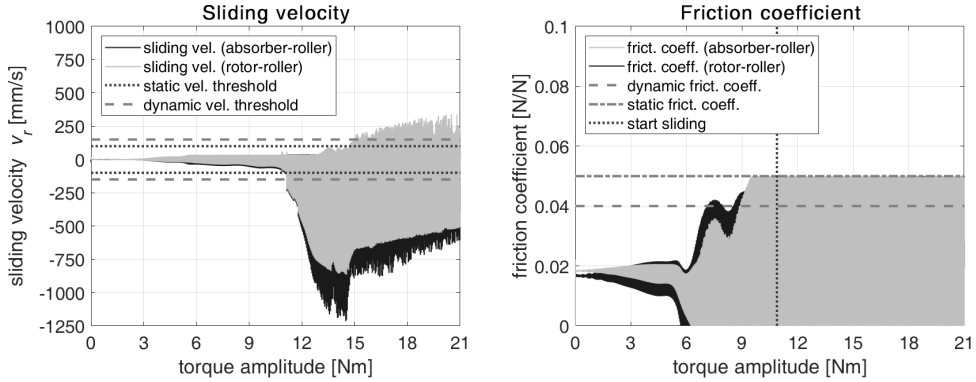

Figure 3: sliding velocity (left) and friction coefficient (right) .vs. torque amplitude .

From these plots, the following considerations arise:

- For low torque values, the sliding velocity is close to zero, which means that the pure-rolling condition is satisfied completely, due to stiction.
- For medium torque levels, there is a finite sliding velocity, but its value is less than the threshold velocity. Hence, the rolling condition is still valid.
- For high torque amplitudes, the sliding velocity is greater than the threshold and the friction coefficient reaches the dynamic value. In these cases, there is slipping between the roller and the slot.

However, observing Figure 5, which is the zoom versions of Figure 3, the slipping is only localized at the end of the time period of oscillation.

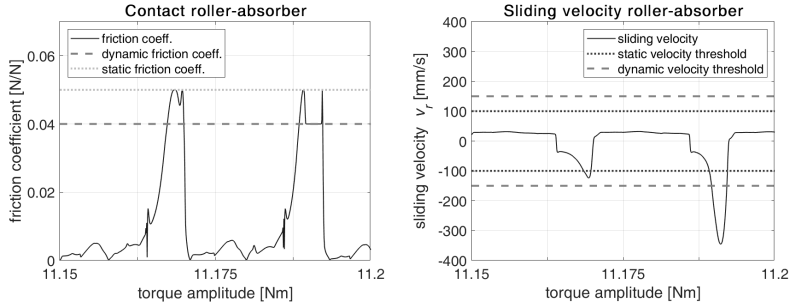

Figure 5: sliding velocity and friction coefficient .vs. torque amplitude (zoom version)

To assess the power losses due to the roller-slot slipping, the ratio between friction power loss of all the caged-roller joints and disturbance power *FP/DP*:

$$\frac{FP}{DP} = \frac{\int_{-\pi}^{\pi} \sum_{i=1}^{8} F_t v_r \mathrm{d}\Theta}{\int_{-\pi}^{\pi} T\Omega \sin n\Theta \mathrm{d}\Theta} \tag{9}$$

averaged over a period is computed. This ratio is plotted with respect to the torque amplitude in Figure 6. As expected, since the slipping is very limited, the power loss is negligible even for large oscillations.

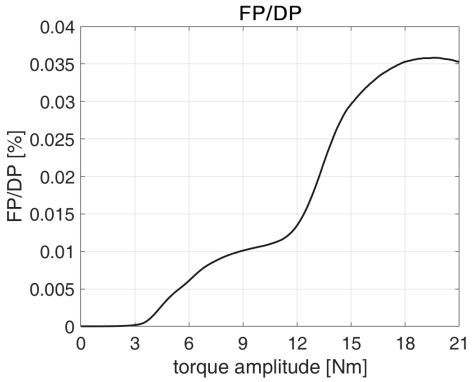

Figure 6: ratio *FP/DP* .vs. torque amplitude

Conclusions

In this investigation, the internal dynamics of the caged-roller joints of a centrifugal pendulum is analyzed by means of the multibody environment. In the caged-roller joints, the pure-rolling between the mating elements is required. However, as observed in the multibody dynamics simulations, there could be slipping for large absorber oscillations. This occurs mostly for low rotor speed, when the centrifugal force field amplitude is not enough to guarantee a sufficient normal force between the roller and the slot throughout the entire oscillation. To assess the power losses associated with this phenomenon, the ratio between the friction and the disturbance powers is computed. From this comparison, the friction power losses are negligible for any oscillations.

References

[1] A. Kooy and R. Seebacher. Best-in-class dampers for every driveline concept. Schaeffler Symposium, (2018)

[2] J. P. Den Hartog. Mechanical vibrations, fourth edition. J. R. Aeronaut. Soc. 61 (554) (1957).

[3] H.H. Denman, Tautochronic bifilar pendulum torsion absorbers for reciprocating engines, J. Sound Vib. 159 (2) (1992). https://doi.org/10.1016/0022-460X(92)90035-V

[4] C.P. Chao, S.W. Shaw, C.T. Lee, Stability of the unison response for a rotating system with multiple tautochronic pendulum vibration absorbers, J. Appl. Mech. 64 (1) (1997) 149–156. https://doi.org/10.1115/1.2787266

[5] A.S. Alsuwaiyan and S.W. Shaw. Performance and dynamic stability of general-path centrifugal pendulum vibration absorbers. J. Sound Vib., 252(5) (2002). https://doi.org/10.1006/jsvi.2000.3534

[6] J. Mayet, H. Ulbrich, First-order optimal linear and nonlinear detuning of centrifugal pendulum vibration absorbers, J. Sound Vib. 335 (2015) 34–54. https://doi.org/10.1016/j.jsv.2014.09.017

[7] M. Cirelli, M. Cera, E. Pennestrì, P.P. Valentini, Nonlinear design analysis of centrifugal pendulum vibration absorbers: an intrinsic geometry-based framework, Nonlinear Dynam. 102 (3) (2020) 1297–1318. https://doi.org/10.1007/s11071-020-06035-1
[8] M. Cera, M. Cirelli, E. Pennestrì, and P. P. Valentini. Design analysis of torsichrone centrifugal pendulum vibration absorbers. Nonlinear Dynam. 104 (2) (2021) 1023–1041. https://doi.org/10.1007/s11071-021-06345-y
[9] M. Cera, M. Cirelli, E. Pennestrì, P.P. Valentini, Nonlinear dynamics of torsichrone CPVA with synchroringed form closure constraint, Nonlinear Dynam.105 (3) (2021) 2739–2756. https://doi.org/10.1007/s11071-021-06732-5
[10] E.R. Gomez, I.L. Arteaga, L. Kari, Normal-force dependent friction in centrifugal pendulum vibration absorbers: Simulation and experimental investigations, J. Sound Vib. 492 (2021). https://doi.org/10.1016/j.jsv.2020.115815
[11] O. Bauchau, J. Rodriguez, and S.Y. Chen. Modeling the bifilar pendulum using nonlinear, flexible multibody dynamics. J. American Helicopter Society 48 (2003). https://doi.org/10.4050/JAHS.48.53
[12] M. Cera, M. Cirelli, E. Pennestrì, P.P. Valentini, The kinematics of curved profiles mating with a caged idle roller - higher-path curvature analysis, Mech. Mach. Theory 164 (2021). https://doi.org/10.1016/j.mechmachtheory.2021.104414
[13] J. Mayet, Effective and robust rocking centrifugal pendulum vibration absorbers, J. Sound Vibr. 527 (2022). https://doi.org/10.1016/j.jsv.2022.116821
[14] M. Cera, M. Cirelli, E. Pennestrì, P.P. Valentini, Design and comparison of centrifugal dampers modern architectures: The influence of roller kinematics on tuning conditions and absorbers nonlinear dynamics, Mech. Mach. Theory 174 (2022). https://doi.org/10.1016/j.mechmachtheory.2022.104876
[15] P. Flores, Contact mechanics for dynamical systems: a comprehensive review. Mult. Syst. Dynam., 54(2) (2021). https://doi.org/10.1007/s11044-021-09803-y
[16] C. M. Pereira, A. L. Ramalho, J. A. Ambrósio, A critical overview of internal and external cylinder contact force models, Nonlinear Dynam. 63 (2011). https://doi.org/10.1007/s11071-010-9830-3
[17] M. Cera, E. Pennestrì, The mechanical generation of planar curves by means of point trajectories, line and circle envelopes: a unified treatment of the classic and generalized Burmester problem, Mech. Mach. Theory 142 (2019). https://doi.org/10.1016/j.mechmachtheory.2019.103580
[18] F. Freudenstein, L.S. Woo, On the curves of synthesis in plane instantaneous kinematics, in: M. Hetényi, W.G. Vincenti (Eds.), Applied Mechanics. International Union of Theoretical and Applied Mechanics, Springer (1969)
[19] J. Choi, H. S. Ryu, C. W. Kim, and J. H. Choi. An efficient and robust contact algorithm for a compliant contact force model between bodies of complex geometry. Mult. Syst. Dynam., 23(1) (2009). https://doi.org/10.1007/s11044-009-9173-3
[20] H. Y. Cha, J. Choi, H. S. Ryu, and J. H. Choi. Stick-slip algorithm in a tangential contact force model for multi-body system dynamics. J. Mech. Science and Technology, 25(7) (2011). https://doi.org/10.1007/s12206-011-0504-y
[21] E. Pennestrì, V. Rossi, P. Salvini, and P. P. Valentini. Review and comparison of dry friction force models. Nonlinear Dynam., 83(4) (2015). https://doi.org/10.1007/s11071-015-2485-3